Monthly Notices
of the
ROYAL ASTRONOMICAL SOCIETY

MNRAS **469,** S142–S148 (2017)
Advance Access publication 2017 June 13

doi:10.1093/mnras/stx1472

Effective ion speeds at ∼200–250 km from comet 67P/Churyumov–Gerasimenko near perihelion

E. Vigren,[1⋆] M. André,[1] N. J. T. Edberg,[1] I. A. D. Engelhardt,[1,2] A. I. Eriksson,[1] M. Galand,[3] C. Goetz,[4] P. Henri,[5] K. Heritier,[3] F. L. Johansson,[1,2] H. Nilsson,[6] E. Odelstad,[1,2] M. Rubin,[7] G. Stenberg-Wieser,[6] C.-Y. Tzou[7] and X. Vallières[5]

[1]*Swedish Institute of Space Physics Uppsala, SE-751 21 Uppsala, Sweden*
[2]*Department of Physics and Astronomy, Uppsala University, SE-751 21 Uppsala, Sweden*
[3]*Department of Physics, Imperial College London, London SW7 2AZ, UK*
[4]*Institute for Geophysics and Extraterrestrial Physics, Technische Universität Braunschweig, D-38106 Braunschweig, Germany*
[5]*Laboratoire de Physique et Chimie de l'Environnement et de l'Espace, F-45071 Orléans Cedex 2, France*
[6]*Swedish Institute of Space Physics Kiruna, SE-981 28 Kiruna, Sweden*
[7]*Physikalisches Institut, University of Bern, CH-3012 Bern, Switzerland*

Accepted 2017 June 9. Received 2017 May 29; in original form 2017 March 31

ABSTRACT

In 2015 August, comet 67P/Churyumov–Gerasimenko, the target comet of the ESA *Rosetta* mission, reached its perihelion at ∼1.24 au. Here, we estimate for a three-day period near perihelion, effective ion speeds at distances ∼200–250 km from the nucleus. We utilize two different methods combining measurements from the Rosetta Plasma Consortium (RPC)/Mutual Impedance Probe with measurements either from the RPC/Langmuir Probe or from the *Rosetta Orbiter Spectrometer for Ion and Neutral Analysis* (*ROSINA*)/Comet Pressure Sensor (COPS) (the latter method can only be applied to estimate the effective ion drift speed). The obtained ion speeds, typically in the range 2–8 km s^{-1}, are markedly higher than the expected neutral outflow velocity of ∼1 km s^{-1}. This indicates that the ions were de-coupled from the neutrals before reaching the spacecraft location and that they had undergone acceleration along electric fields, not necessarily limited to acceleration along ambipolar electric fields in the radial direction. For the limited time period studied, we see indications that at increasing distances from the nucleus, the fraction of the ions' kinetic energy associated with radial drift motion is decreasing.

Key words: molecular processes – comets: individual: 67P/Churyumov–Gerasimenko.

1 INTRODUCTION

Comet 67P/Churyumov–Gerasimenko, hereafter 67P, is a Jupiter-family comet with an orbital period of 6.44 yr and with aphelion and perihelion at ∼5.68 and ∼1.24 au, respectively. It was the target comet of the ESA *Rosetta* mission, which studied the comet up-close for a period of more than 2 yr, from 2014 July to 2016 September with a perihelion passage in 2015 August. The varying activity level of the comet was probed by different means as described in Hansen et al. (2016). One method makes use of measurements of the neutral number density, n_N, from the Rosetta Orbiter Spectrometer for Ion and Neutral Analysis - Comet Pressure Sensor (*ROSINA*/COPS, see Balsiger et al. 2007). Combined with an estimate of the expansion velocity (typically in the range ∼0.5–1 km s^{-1}; e.g. Hansen et al. 2016) and the assumption of a $1/r^2$ decay in the neutral number density (r is cometocentric distance), such measurements give an estimate of the comet's outgassing rate Q (note, however, that this is a local estimate and that the global outgassing rate across the surface of the comet may differ from such estimates).

Ions produced by photoionization can be assumed to initially have the same velocity (magnitude and direction) as the neutrals they stemmed from because the bulk of the excess energy of the process goes into kinetic energy of the ejected electrons. The ions are then subject to electromagnetic fields and can be accelerated as well as deflected, but as long as collisions with the neutrals are frequent enough, the ion velocity will remain close to the neutral velocity; i.e. the ions are *collisionally coupled* to the neutrals. The ion-neutral de-coupling distance, r_{IN}, is based on comparisons of collision- and transport time-scales, expected roughly at (Gombosi 2015):

$$r_{IN} = \frac{k_{IN} Q}{4\pi u^2}, \quad (1)$$

⋆ E-mail: erik.vigren@irfu.se

where k_{IN} is the ion-neutral charge exchange rate coefficient [referring to the work Cravens & Körözmezey (1986), Gombosi (2015), suggests $k_{IN} \approx 1.1 \times 10^{-9}$ cm^3 s^{-1}], Q is the outgassing rate and u the neutral outflow velocity. Mandt et al. (2016) use a different expression to estimate the collisionopause location (inwards of which collisions between plasma and neutrals dominate the plasma dynamics):

$$r_{IN} = \sigma_{IN}\, n_{N,sc} r_{sc}^2. \quad (2)$$

Here, σ_{IN} is a momentum transfer cross-section for which Mandt et al. (2016) considered values in the range (2–8) $\times$ 10^{-15} cm^2, and $n_{N,sc}$ is the neutral number density measured at the spacecraft location r_{sc}. It is noted that equation (2) is the solution to the equation $\lambda(r) = r$, where λ is the local mean free path of ions and where it is assumed that the neutral number density decays as $1/r^2$.

Making assumptions of collisionally coupled ions ease some of the complexity of ionospheric modelling as the influence of electromagnetic fields then is neglected. With an ion flow speed equal to neutral outflow velocity, $u_{I,flow} = u$, analytical expressions for how the number density of ions, n_I, vary with $r < r_{IN}$ can be derived. A simple model, which assumes a constant ionization frequency, ν, and negligible plasma loss through dissociative recombination, yields for example (e.g. Galand et al. 2016; Vigren et al. 2016):

$$n_I\ (r) = \frac{Q\nu \times\ (r - r_c)}{4\pi u^2 r^2} \quad (3)$$

where r_c is the cometary radius and the other parameters are as described above. For $r \gg r_{sc}$, it is seen that n_I is following a $1/r$ relation. Such a dependence of the plasma density was in fact observed during radial scans in the early escort phase of the *Rosetta* mission, although with large variations indicative of a highly dynamic plasma (Edberg et al. 2015). A model, which in addition accounts for dissociative recombination, though with the assumption of a constant effective recombination coefficient, gives the analytical expression for n_I versus r given by equation (12) in Gombosi (2015). The equation is not repeated here but contains also a $1/r$ dependence.

Recently, Vigren & Eriksson (2017) developed a 1D model to test the ability of H_2O molecules to interrupt ion acceleration along weak electric fields in the radial direction. From the model results, they raised concerns about the correctness in assuming $u_{I,flow} = u$ for $r < r_{IN}$ as given by Equation (1) or (2). As an example, for perihelion conditions, r_{IN} from equation (1) is at ~1000 km, while the estimated effective ion flow speed at 200 km was calculated as several km s^{-1}, assuming a rather weak electric field strength of the order of ~0.03–0.1 mV m^{-1}, which may commence due to the electron pressure gradient force. Their finding would support the observations of H_3O^+/H_2O^+ number density ratios observed at times to be lower than predicted by models running with the assumption of collisionally coupled ions (see fig. 7 of Fuselier et al. 2016). The observed ratios were observed to be variable and at times also at the level predicted by collisionally coupled models (see in particular, Fig. 6 of Fuselier et al. 2016), particularly so when the RPC-Ion Electron Sensor (RPC-IES, see Mandt et al. 2016) did not see clear signs of ion acceleration. Vigren & Eriksson (2017) referred also to preliminary values of effective ion speeds (not restricted to ion flow speeds) of several km s^{-1} as calculated from combined measurements by the Mutual Impedance Probe (MIP, Trotignon et al. 2007) and the Langmuir Probe (LAP, Eriksson et al. 2007), both being subsystems of the Rosetta Plasma Consortium (RPC, Carr et al. 2007).

In this work, we will first (Section 2) discuss the MIP and LAP measurements and how they can serve to estimate the mean (or rather the effective) ion speed. The selected time interval for the study, 2015 August 2–4, near perihelion, is discussed in Section 3. Results are presented and discussed in Section 4. The derived effective ion speeds are markedly higher than the neutral outflow velocity and also shown to at least periodically be in good agreement with effective ion drift speeds derived from an independent method; a simple flux conservation model relying on MIP and COPS measurements. The work is briefly summarized in Section 5.

2 METHOD

Our method utilized to derive effective ion speeds is based on combining electron number densities measured by the MIP with voltage–current characteristics from the ion side (negative voltages) of Langmuir probe bias voltage sweeps (we used the LAP1 sensor, see Eriksson et al. 2007 for details).

The MIP measurements consist of determining the mutual impedance between two electric antennas – a transmitting and a receiving one. The transmitting electrode injects an oscillating current in the plasma, at a given frequency, while the receiving one measures the potential difference induced in the plasma at the same frequency. The frequency is increased step by step, in a frequency range that ideally contains the plasma frequency. The electron number density, n_e, is derived from the estimated position of the plasma frequency in the MIP complex (amplitude and phase) mutual impedance spectrum. In this paper, we are focusing on a rather high activity period near perihelion (2015 August 2–4) when MIP was operated in the Short Debye Length mode using the MIP sensor alone (when operated in the Long Debye Length mode the MIP experiment makes use of LAP2 as a transmitter).

For a drifting Maxwellian distribution, the ion current, I, to a spherical Langmuir probe at bias voltage U can (with standard sign conventions for Langmuir probes) be approximated as (see e.g. Jacobsen et al. 2009, and references therein)

$$I = -4\pi r_{LAP}^2 n_I q \sqrt{\frac{k_B T_I}{2\pi m_I} + \frac{u_{I,drift}^2}{16}} \times \left(1 - \frac{qU}{8m_I\left(\frac{k_B T_I}{2\pi m_I} + \frac{u_{I,drift}^2}{16}\right)}\right), \quad (4)$$

where r_{LAP} is the radius of the Langmuir probe (=2.5 cm), q is the elementary charge, n_I is the ion number density, m_I is the ion mass (we assume 19 amu, the mass of an H_3O^+ ion), k_B is Boltzmann's constant, $u_{I,drift}$ is the drift velocity of ions and T_I is the ion temperature. If we define an *effective ion velocity*, u_I, according to

$$u_I = \sqrt{\frac{8k_B T_I}{\pi m_I} + u_{I,drift}^2}, \quad (5)$$

then equation (4) can be simplified and differentiated as to yield

$$\frac{dI}{dU} = \frac{q^2 n_I A_{LAP}}{2m_I u_I}, \quad (6)$$

where $A_{LAP} = 4\pi r_{LAP}^2$ is the surface area of the Langmuir probe and u_I is the effective ion speed defined by equation (5). If the scenario of collisionally coupled and cold ions would hold true, then the u_I values derived from equation (6) would be expected close to ~1 km s^{-1}, i.e. close to the neutral flow speed (see e.g. Hansen et al. 2016; Heritier et al. 2017). To assess u_I, we assume charge neutrality and replace n_I in equation (6) by n_e as measured

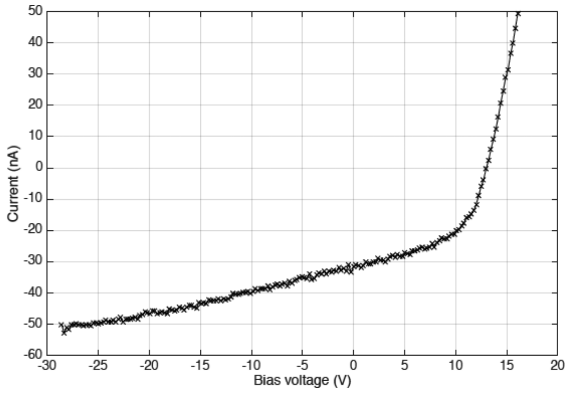

Figure 1. Current versus bias voltage sweep from LAP1 bias voltage sweep conducted 2015 August 2, UT: 10.03.44. The slope d*I*/d*U* on the ion side (negative voltage) is in this case 0.64 nA/V.

by MIP. The slope d*I*/d*U* is obtained from LAP bias voltage sweeps with an example given in Fig. 1.

The described approach may yield overestimated ion flow speeds, and are expected to do so when the Debye length is long enough and the probe resides within the potential field of the negatively charged spacecraft. Under such circumstances, ions will experience some pre-acceleration yielding somewhat underestimated d*I*/d*U* and therefore overestimated u_I, should the electron number density measurements obtained from MIP not also be influenced by the potential field of the spacecraft. From LAP measurements of the photoelectron knee potential (see Odelstad et al. 2015) and ion spectra measured by the RPC/Ion Composition Analyzer (ICA, Nilsson et al. 2007), efforts are currently undertaken to establish the fraction of the spacecraft potential that resided outside the probe location at different stages of the *Rosetta* mission. In addition, simulations using the Spacecraft Plasma Interaction System are currently conducted, as an extension of the work by Johansson et al. (2016), to establish the effects of the spacecraft charging on plasma parameters. Here, we are merely raising concerns of these effects though noticing that 5 eV electrons at a density of ∼1000 cm^{-3} correspond to a Debye length of ∼0.5 m, which is shorter than the boom on which MIP and LAP1 are mounted (for example, for LAP1 the distance from hinge to the probe is 2.24 m, see Eriksson et al. 2007). We also find that the derived effective ion speeds are not in severe conflict with effective ion drift speeds derived from an independent method consisting of a simple flux conservation model driven by neutral number densities as measured by *ROSINA*/COPS (see further Section 4).

3 CONDITIONS DURING INVESTIGATED TIME PERIOD

Here, we give brief information on geometrical parameters associated with the investigated time period of 2015 August 2–4. For context, we describe also some features of the plasma and magnetic field environment during this time. In Fig. 2(a), we show how the cometocentric distance of *Rosetta* varied throughout the three-day period with a minimum distance of ∼207 km and a maximum distance of ∼251 km. Fig. 2(b) shows the latitudinal and longitudinal coverage as well as the solar aspect angle. The variation in longitude reflects primarily the rotation period of the comet (∼12 h). The spacecraft resided at southern latitudes, at that time the summer side of the comet, and close to the terminator. To maximize power output, the solar panels were almost always held perpendicular to the solar direction. This means, the illumination of surfaces on the spacecraft body was determined by only one angle, the solar aspect angle. This is defined as the angle between the Sun and the spacecraft +Z axis (see e.g. Fig. 1 in Johansson et al. 2017), counted positive toward the spacecraft +X axis. As +Z is the pointing direction of, for example, all imaging instruments on *Rosetta*, this axis was typically pointing to the nucleus. As a consequence, the typical value of the solar aspect angle in terminator orbit was +90°. It is seen that the spacecraft was turned in such a way that the solar aspect angle changed considerably during several hours on August 3 and 4, which we return to in Section 4. Fig. 2(c) shows the photoelectron knee potential measured by LAP1 (see Odelstad et al. 2015), the negative of which would correspond to the spacecraft

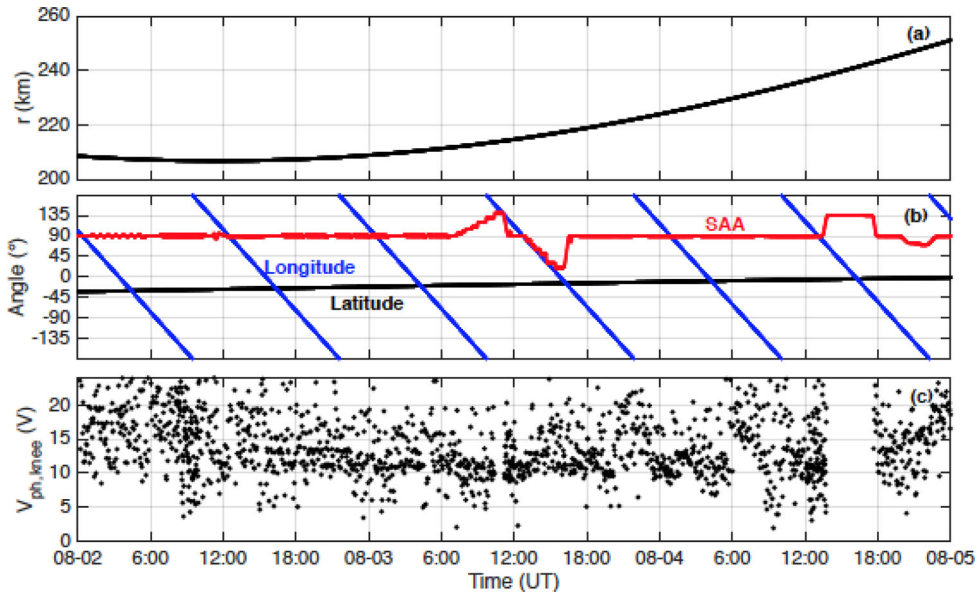

Figure 2. Shown against time (UT on 2015 August 2–4) are (a) the cometocentric distance of *Rosetta*, (b) the latitude (changing from –32° to –1° over the studied time interval) and longitude of *Rosetta*, as well as the solar aspect angle (SAA), (c) the photoelectron knee potential derived from bias voltage sweeps of the LAP1 sensor.

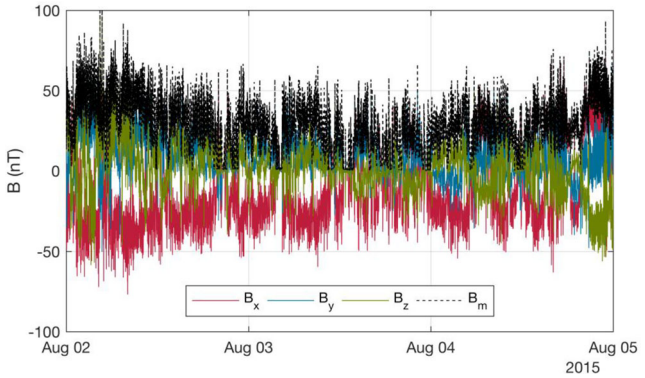

Figure 3. Magnetic field magnitude and components from MAG measurements. B is given in the body-centred solar equatorial frame (CSEQ), where x points towards the Sun, z is along the part of the Sun's North Pole that is orthogonal to the ecliptic and y completes the right-handed coordinate system. The diamagnetic cavity is visible as short intervals of zero field strength starting on the evening of August 2. Otherwise, the B_x component is dominating, and mostly negative, although it switches directions for some shorter intervals.

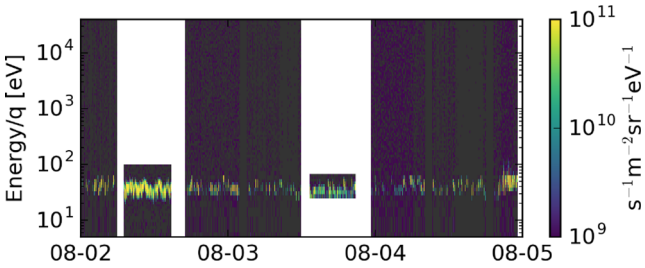

Figure 4. Ion energy spectrograms summed over all viewing directions as derived from ICA measurements during 2015 August 2–4. Empty regions (dark grey or white) indicate lack of measurements or measurements over more limited energy intervals.

potential provided that the probe is not well within the potential field of the spacecraft. Throughout the investigated time period, the spacecraft remained negatively charged but with substantial variation in the –5 to –20 V range reflecting a highly dynamic plasma environment.

During the investigated time, the average magnetic field strength as measured by the RPC Magnetometer (MAG, Glassmeier et al. 2007), was around 30 nT, although for a couple of hours at beginning and end, the magnitude was slightly higher, ∼50nT (see Fig. 3). The field was mostly oriented with a ∼40° angle from the comet–sun line. There are several short intervals where the magnetic field vector changed orientation. From the evening of August 2 there are short, intermittent intervals of zero magnetic field magnitude, the longest of which is ∼30 min. This indicates the diamagnetic cavity reaching out to *Rosetta* at these times (Goetz et al. 2016a,b; Henri et al. 2017). On shorter scales, the magnetic field is dominated by one-sided steepened waves (Stenberg-Wieser et al. 2017) that are typical for the plasma just outside the diamagnetic cavity.

The ion observations by ICA made on August 2–4 (ion spectrogram shown in Fig. 4) were dominated by a low-energy population of cometary (water group) ions, with the negatively charged spacecraft accelerating positive ions into the ion detector. The spacecraft potential varied substantially, see Fig. 2(c) (on the order of 20 V) on a time-scale of minutes and most of the apparent energy variations in the ion data reflect this. The energy width (temperature) of the ion population did not vary much and was on the order of a few to 10 eV. No accelerated cometary ion population (cometary ions at hundreds of eV, see e.g. Nilsson et al. 2015, 2017) was observed, and also there were no observations of solar wind ions during this period, suggesting that the spacecraft resided in a solar wind void surrounding the comet (Nilsson et al. 2015; Behar et al. 2016).

4 RESULTS AND DISCUSSION

In Fig. 5(a), we show how the neutral number density at the spacecraft location varied over the investigated 3-d period. The displayed data have been corrected for a constant background level and we have assumed that the composition is purely H_2O (see Galand et al. 2016 for more information on COPS measurements and associated corrections). The general trend of decreasing neutral number densities reflects primarily the increasing latitude and cometocentric distance (see Fig. 2a). There is also a ∼12 h variation associated with non-uniform outgassing and nucleus rotation. In addition, some features are related to spacecraft manoeuvres, including off-pointing. These include the most noticeable feature in the displayed data; namely the (apparently) enhanced neutral number densities around 12:00 and a few hours forward on August 3, which is not reflecting a change in the cometary activity but is related to the large off-pointing slew visible in the solar aspect angle in Fig. 2(b). Large off-pointing slews can expose previously cold surfaces of the spacecraft to the sun and thus lead to the release of trapped volatiles.

In Fig. 5(b), we show the electron number densities obtained from the MIP experiment (see Section 2), revealing short scale high plasma density variations. Fig. 5(c) shows the values of dI/dU as fitted for LAP bias voltage sweeps (see Fig. 1). The n_e ($n_e = n_I$) and dI/dU data are combined (equation 6) to give the estimated effective ion speeds, u_I, as shown by the red crosses in Fig. 5(d). Overplotted by blue dots in the same figure are effective ion drift speeds derived from a simple flux conservation model assuming radial ion outflow. These latter speeds were obtained from the equation (inferred from equation 3 for $r \gg r_C$):

$$u_{I,\mathrm{drift}} \approx \frac{n_{N,sc} r_{sc} \nu}{n_I}, \qquad (7)$$

where $n_{N,\,sc}$ is the neutral number density measured at the spacecraft location, r_{sc} is the cometocentric distance of *Rosetta*, n_I is the ion number density (assumed equal to the electron number density measured by MIP) and ν is the ionization frequency set to a conservative value of 4.5×10^{-7} s^{-1} (corresponding to an H_2O photoionization frequency of $\sim 7 \times 10^{-7}$ s^{-1} at 1 au, see Vigren et al. 2015). It is noted that combining a solar EUV spectrum [based on TIMED/SEE measurements (see Woods et al. 2005) and extrapolated in distance and phase to the location of *Rosetta* on 2015 August 3] with H_2O photoionization cross-sections from Schunk & Nagy (2009) gives a photoionization frequency of 3.96×10^{-7} s^{-1}. With an additional 10 per cent ionization by photoelectrons (reasonable based on the calculations of Vigren & Galand 2013), our utilized ionization frequency is justified.

Note that in contrast to the speed derived by use of equation (6), the speed from equation (7) is a flow speed, with no contribution from any possible thermal spread. It is stressed that thermal motion or wave associated motion of the ions would not alter the appearance of equation (7) as such motions to first order are not expected to strongly influence the flux divergence. Somewhat overestimated values can be expected due to the neglect of EUV attenuation and plasma loss through dissociative recombination, but the overestimation is unlikely to exceed a few tens of per cent unless electron cooling is very efficient over a significant part of the coma (see

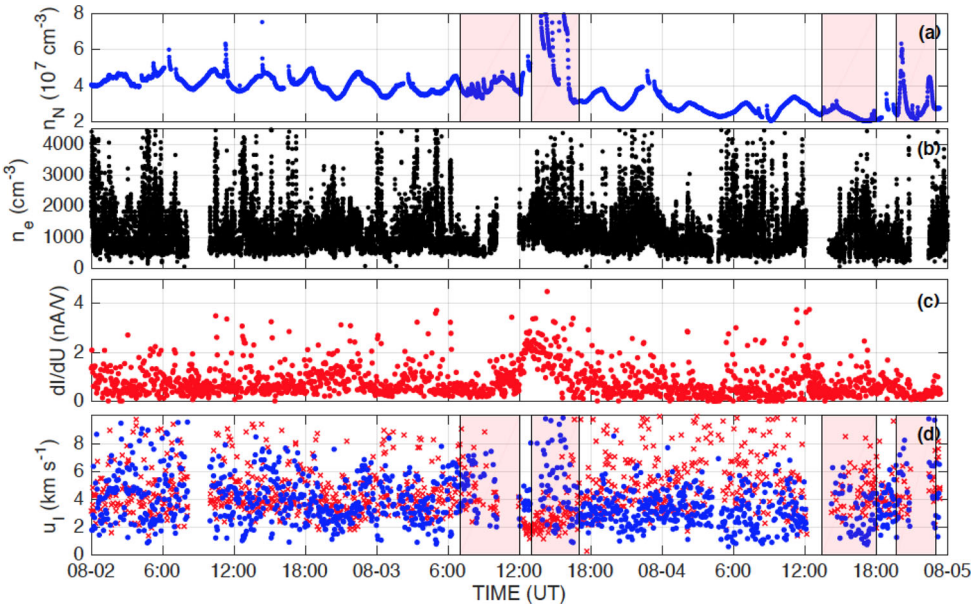

Figure 5. Shown against time (UT on 2015 August 2–4) are (a) neutral number densities measured by *ROSINA*/COPS, (b) electron number densities measured by RPC/MIP, (c) d*I*/d*U* observed during bias voltage sweeps by RPC/LAP, and (d) computed effective ion drift speeds from equation (7) (based on data in panels a and b and shown by blue dots) and effective ion speeds from equation (6) (based on data in panels b and c and shown by red crosses). Pink shaded regions are associated with times when the solar aspect angle was varying and departed from ∼90°. The data within these boxes are unreliable, in particular, the blue data points within the second and fourth pink box from the left as these correspond to times when the side of the spacecraft on which COPS is mounted was illuminated (associated increase in spacecraft outgassing from the deck close to COPS).

Vigren et al. 2015) and unless pronounced EUV absorption/scattering by grains commences inwards of the spacecraft location. It is noted that LAP can be used as an EUV monitor and that observations over the full escort phase of the *Rosetta* mission, including comparisons to fluxes expected based on e.g. extrapolated TIMED/SEE data, indicate non-negligible EUV damping at the spacecraft location when near perihelion (well exceeding the level anticipated from photoabsorption by gas phase molecules alone). An interpretation of this is EUV absorption by submicron grains originating from predominantly upstream splitting of larger grains (see Johansson et al. 2017).

It is seen in Fig. 5(d) that the ion speeds derived from the two methods are reasonably consistent during August 2 and the first half of August 3, while after the off-pointing slew on August 3 (a time interval during which at least the blue points in Fig. 5d should be ignored) and, in particular, during August 4, the ion speeds derived from equation (6) are higher than the drift speeds obtained from equation (7). This could be an indication of a more heated ion population at further distance from the nucleus with an increasing fraction of the overall energy budget of the ions being in oscillatory motion or thermal motion. Overall, the methods give ion speeds almost exclusively in excess of 2 km s^{-1} and typically in the range 2–8 km s^{-1}. Despite potential adjustments of this range of values (following careful studies of the influence of the negatively charged spacecraft), it appears unlikely that the ions were strongly coupled to the neutrals by the spacecraft location given an expected neutral outflow velocity of ∼1 km s^{-1}. It is worthwhile to point out that with off-radial ion trajectories, the usefulness of equation (7) for estimating effective ion drift speeds becomes questionable. In fact, one may picture more compact as well as less compact source regions in which cases equation (7) would underestimate and overestimate the ion drift speed, respectively.

Our finding that effective ion speeds exceed the neutral flow speed even for distances well within the theorized (from equation 1) ion-neutral decoupling distance is in line with results from Koenders et al. (2015), who conducted hybrid simulations for a comet with an activity of $Q = 5 \times 10^{27}$ s^{-1} at a heliocentric distance of 1.6 au. Their model predicted mean cometary ion speeds in the range 2–6 km s^{-1} already by a cometocentric distance of 75 km, though with the flow pattern being rather off-radial (see their fig. 8). Using similar Q and u values as Koenders et al. (2015), the ion-neutral decoupling distance is from equation (1) calculated at ∼400 km using $k_{IN} = 1.1 \times 10^{-9}$ cm^3 s^{-1} (note that Koenders et al. 2015, used $k_{IN} = 1.7 \times 10^{-9}$ cm^3 s^{-1}) and from equation (2) at ∼80–320 km (considering the same cross-section limits as Mandt et al. 2016).

An interesting rise in d*I*/d*U* is seen coinciding with the off-pointing slew near noon on August 3. Here, the ion velocities as deduced from equation (6) (red crosses in Fig. 5d) are the lowest throughout the investigated time period and essentially clumped at values around 2 km s^{-1}. Why d*I*/d*U* would be sensitive to off-pointing is not obvious and requires dedicated follow-up investigations.

We note that between UT 20:32:44 and 20:41:02 on 2015 August 2, the spacecraft resided within the diamagnetic cavity of the comet as attested from MAG measurements (see Goetz et al. 2016a, for more on observations of diamagnetic cavity crossings). The estimated ion speeds from equation (6), displayed by red crosses in Fig 6(d) (only a few points due to the 160 s cadency of the bias voltage sweeps), remained high at values of 3–4 km s^{-1} across this time interval and are fairly close to the effective ion drift speeds estimated from equation (7) and shown by blue circles in Fig. 5(d). Due to the absence of plasma-magnetic field acceleration in the unmagnetized region, it seems plausible that these high ion speeds could be a result of acceleration along an ambipolar electric field set up by the electron pressure gradient. The behaviour of the thermal electron density during diamagnetic cavity crossings is discussed thoroughly in Henri et al. (2017). Typically, the electron number density is

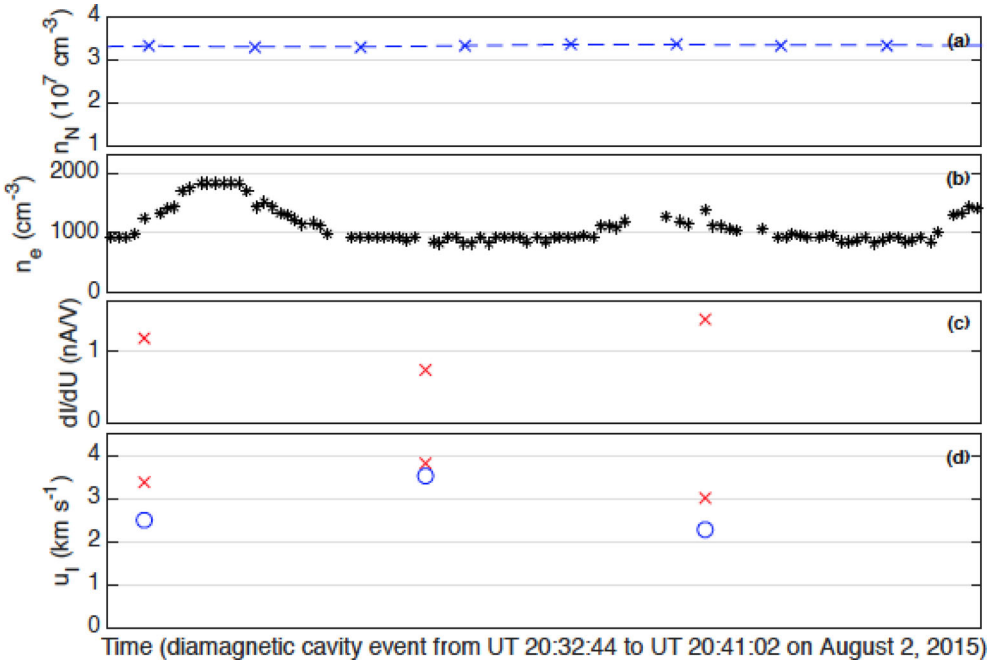

Figure 6. Similar as Fig. 5 but zoomed into a time interval associated with a diamagnetic cavity crossing on 2015 August 2. The COPS measurements are denoted by blue crosses in panel a. The blue circles in panel (d) are ion drift speed estimates based on data interpolated from panel (a) and (b) via equation (7).

found not to vary much during each diamagnetic region crossing. However, Henri et al. (2017) reported that smooth variations in the electron number density are observed in about 15 per cent of the diamagnetic regions crossings. Their origin is still unknown and under study. The crossing displayed in Fig. 6 is an example where such a smooth variation is observed, though for most of the time, the electron number density was at a nearly constant level of 1000 cm^{-3}. It is also noted that the electron number densities observed typically during the diamagnetic cavity crossings are not compatible with ion drift speeds at a level much higher than ∼3 km s^{-1} or so (cf. equation 7 and Henri et al. 2017). This indicates that effective ion drift speeds near 8 km s^{-1} (seen occasionally in Fig. 5d) are likely associated with plasma-magnetic field acceleration outside the cavity.

When considering an extended dataset for the whole of 2015 August, the calculated ion speeds from equation (6) vary a lot and with speeds occasionally up to several tens of km s^{-1}. We have binned the calculated ion speeds for the whole of August into groups of 20 (40) and assigned not-a-number to data points for which no MIP derived n_e values were present within less than 30 s from the sweep time. Groups with more than 10 (20) not-a-number entries were discarded and median values were calculated for the rest. The mean of these median values and the standard deviation of this mean are 6.1 and 3.2 km s^{-1}, respectively (5.9 and 3.0 km s^{-1}, respectively). For the 3-d period, August 2–4, primarily focused on in this paper, the corresponding numbers are 5.5 and 1.5 km s^{-1}, respectively, for the mean and its standard deviation (regardless of considering groupings of 20 or 40 sweep times). Effective ion drift speeds derived from equation (7) for the whole of 2015 August are as expected lower (mean of 3.3 km s^{-1}) and are periodically even at the level of the expected neutral outflow speed. We will return to this in a later study.

We note finally that Beth et al. (2016), based on near perihelion *ROSINA*/DFMS measurements reported on the first detection of NH_4^+ in a cometary coma and at abundances comparable to that of water group ions. The effective ion drift speeds derived at the spacecraft location in this work would not fit well with such high relative abundances of NH_4^+, if applied as the outward ion speed throughout the coma in an ionospheric model. However, the influence of a variable electric field on ion number density ratios is not straightforwardly assessed. As an example, over a region of a strong outward electric field, the ratios of ions of roughly similar mass-to-charge ratios and both relying on ion–neutral interactions for production (e.g. H_3O^+ from $H_2O^+ + H_2O$ and NH_4^+ from $H_3O^+ + NH_3$) would likely not undergo much of a change due to the reduced proton transfer cross sections with increased relative velocity with respect to the surrounding neutrals (which in turn are unaffected by the field).

5 SUMMARY AND CONCLUDING REMARKS

We have combined measurements from LAP and MIP as well as from COPS and MIP in order to estimate effective ion speeds at distances ∼200–250 km from the nucleus of comet 67P/Churyumov–Gerasimenko, while near perihelion in early August of 2015. The methods give effective ion speeds (or effective ion drift speeds) typically in the range of 2–8 km s^{-1} and well above the expected neutral outflow velocity of ∼1 km s^{-1}. This favours that the ions were collisionally de-coupled from the neutrals by the spacecraft location during this time interval. When moving towards greater cometocentric distances, or more generally towards regions of lower neutral number densities, we see at least indications of a growing fraction of the ions' energy prevailing in thermal, oscillatory (plasma wave related) or non-radial motion. We plan to extend this study to the whole escort phase of the *Rosetta* mission, though alerting that the applicability of our method becomes more questionable when ambient electron number densities goes down and the Debye length increases. From inspection of data for the whole of 2015 August, there are marked variations in the effective ion speeds derived from our two approaches. The estimated ion drift speed remains, as

expected, lower than the effective ion speed (which in addition to drift motion include also thermal/oscillatory motion), but is periodically at comparable levels and periodically reduced to values near the expected outflow velocity of the neutrals. This will be further investigated and reported in detail in a future study.

ACKNOWLEDGEMENTS

Rosetta is a European Space Agency (ESA) mission with contributions from its member states and the National Aeronautics and Space Administration (NASA). We are indebted to the whole of the *Rosetta* Mission Team, the Rosetta Science Ground Segment (SGS) and the Rosetta Mission Operations Centre (RMOC) for their outstanding efforts in making this mission possible. Work at the Swedish Institute of Space Physics are funded by the Swedish National Space Board (contracts 109/02, 135/13, 166/14, and 114/13) and the Swedish Research Council (621–2013-4191 and 621–2014-5526). Work on *ROSINA*/COPS at the University of Bern was funded by the State of Bern, the Swiss National Science Foundation and the ESA PRODEX Program. The work on RPC-MAG was financially supported by the German Ministerium für Wirtschaft und Energie and the Deutsches Zentrum für Luft- und Raumfahrt under contract 50QP 1401. Work at LPC2E/CNRS was supported by Exploration spatiale des environments planétaires (ESEP), Centre national d'études spatiales (CNES) and by Agence Nationale de la Recherche (ANR) under the financial agreement ANR-15-CE31–0009-01. Work at Imperial College London is supported by Imperial College President's scholarship and the Science and Technology Facilities Council (STFC) of UK under grants ST/K001051/1 and ST/N000692/1. We thank a reviewer for valuable comments.

REFERENCES

Balsiger H. et al., 2007, Space Sci. Rev., 128, 745
Behar E., Lindkvist J., Nilsson H., Holmström M., Stenberg-Wieser G., Ramstad R., Götz C., 2016, A&A, 596, A42
Beth A. et al., 2016, MNRAS, 462, S562
Carr C. et al., 2007, Space Sci. Rev., 128, 629
Cravens T. E., Körosmezey A., 1986, P&SS, 34, 961
Edberg N. J. T. et al., 2015, Geophys. Res. Lett., 42, 4263
Eriksson A. I. et al., 2007, Space Sci. Rev., 128, 729
Fuselier S. A. et al., 2016, MNRAS, 462, S67
Galand M. et al., 2016, MNRAS, 462, S331
Glassmeier K.-H. et al., 2007, Space Sci. Rev., 128, 649
Goetz C. et al., 2016a, MNRAS, 462, S459
Goetz C. et al., 2016b, A&A, 588, A24
Gombosi T. I., 2015, in Kelling A., Jackman C.M., Delamere P.A., eds, Magnetotails in the Solar System. Wiley, Hoboken, NJ, p. 169
Hansen K. C. et al., 2016, MNRAS, 462, S491
Henri P. et al., 2017, MNRAS, in press
Heritier K. et al., 2017, MNRAS, in press
Jacobsen K. S., Wahlund J. E., Pedersen A., 2009, P&SS, 57, 48
Johansson F., Henri P., Eriksson A., Vallières X., Lebreton J.-P., Béghin C., Wattieaux G., Odelstad E., 2016, in Proc. 14th Spacecraft Charging Technology Conference, Simulations of the Rosetta Spacecraft Interaction with Comet Plasma. ESA/ESTEC Noordwijk
Johansson F. L. et al., 2017, MNRAS, in press
Koenders C., Glassmeier K.-H., Richter I., Ranocha H., Motschmann U., 2015, P&SS, 105, 101
Mandt K. E. et al., 2016, MNRAS, 462, S9
Nilsson H. et al., 2007, Space Sci. Rev., 128, 671
Nilsson H. et al., 2015, A&A, 583, A20
Nilsson H. et al., 2017, MNRAS, in press
Odelstad E. et al., 2015, Geophys. Res. Lett., 42, 10126
Schunk R. W., Nagy A. F.,, 2009, Ionospheres: Physics, Plasma Physics, and Chemistry (Atmospheric and Space Science Series. Cambridge Univ. Press, Cambridge
Stenberg-Wieser G. et al., 2017, MNRAS, in press
Trotignon J. G. et al., 2007, Space Sci. Rev., 128, 713
Vigren E. et al., 2016, AJ, 152, 59
Vigren E., Galand M., 2013, ApJ, 772, 33
Vigren E., Galand M., Eriksson A. I., Edberg N. J. T., Odelstad E., Schwartz S. J., 2015, ApJ, 812, 54
Vigren E., Eriksson A. I., 2017, AJ, 153, 150
Woods T. N. et al., 2005, J. Geophys. Res., 110, A01312

This paper has been typeset from a Microsoft Word file prepared by the author.